Secular Trends in Global Tides Derived From Satellite Radar Altimetry

Bij de Vaate, I.; Slobbe, D.C.; Verlaan, M.

DOI
10.1029/2022JC018845

Publication date
2022

Document Version
Final published version

Published in
Journal of Geophysical Research: Oceans

JGR Oceans

RESEARCH ARTICLE
10.1029/2022JC018845

Secular Trends in Global Tides Derived From Satellite Radar Altimetry

I. Bij de Vaate[1], D. C. Slobbe[1], and M. Verlaan[2,3]

[1]Civil Engineering and Geosciences, Delft University of Technology, Delft, The Netherlands, [2]Delft Institute of Applied Mathematics, Delft University of Technology, Delft, The Netherlands, [3]Deltares, Delft, The Netherlands

Key Points:

- Satellite altimetry has for the first time been used to assess large scale secular trends in global tides
- Secular trends in the M_2, S_2, O_1, and K_1 tides are observed across the globe, with amplitude changes up to ±1 mm/year
- Global altimetry-derived trends have magnitudes and spatial variability comparable to estimates at tide gauges

Supporting Information:

Supporting Information may be found in the online version of this article.

Correspondence to:

I. Bij de Vaate,
i.bijdevaate@tudelft.nl

Citation:

Bij de Vaate, I., Slobbe, D. C., & Verlaan, M. (2022). Secular trends in global tides derived from satellite radar altimetry. *Journal of Geophysical Research: Oceans*, *127*, e2022JC018845. https://doi.org/10.1029/2022JC018845

Received 11 MAY 2022
Accepted 14 SEP 2022

Abstract Previous studies have demonstrated that tides are subject to considerable changes on secular time scales. However, these studies rely on sea level observations from tide gauges that are predominantly located in coastal and shelf regions and therefore, the large-scale patterns remain uncertain. Now, for the first time, satellite radar altimetry (TOPEX/Poseidon & Jason series) has been used to study worldwide linear trends in tidal harmonic constants of four major tides (M_2, S_2, O_1, and K_1). This study demonstrates both the potential and challenges of using satellite data for the quantification of such long-term changes. Two alternative methods were implemented. In the first method, tidal harmonic constants were estimated for consecutive 4-year periods, from which the linear change was then estimated. In the second method, the estimation of linear trends in the tidal constants of the four tides was integrated in the harmonic analysis. First, both methods were assessed by application to tide gauge data that were sub-sampled to the sampling scheme of the satellites. Thereafter the methods were applied to the real satellite data. Results show both statistically significant decreases and increases in amplitude up to 1 mm/year and significant phase changes up to ∼0.1 deg/year. The level of agreement between altimeter-derived trends and estimates from tide gauge data differs per region and per tide.

Plain Language Summary Tidal predictions are valuable for many purposes, ranging from processing satellite data to coastal engineering. Although tidal constants are often perceived to be stationary in time, earlier studies have shown that tides are subject to changes both on seasonal and long-term time scales. However, these studies mainly concern coastal data and therefore, the processes at open ocean remain unclear. The study behind this paper is the first that uses global satellite data to quantify secular trends in tides, thereby filling in the gaps of earlier work. Results show the changes in tides to be significant, with both decreases and increases in tidal amplitude of the order of several centimeters and phase changes of several degrees over the past decades.

1. Introduction

Knowledge of tides is important for many practical (e.g., marine navigation, fishery, coastal engineering) and scientific purposes. Although tide predictions often treat tidal harmonic constants as stationary over time, considerable changes in tides have been observed on seasonal (e.g., Bij de Vaate et al., 2021; Müller et al., 2014) to long-term timescales (e.g., Müller et al., 2011; Ray, 2016). On the one hand, modifications of the tides can be the result of local processes, such as changes in coastal morphology or altered river flow (Haigh et al., 2020). On the other hand, observed variations in tides have been linked to regional climatic conditions, for example, the extent of sea ice coverage (e.g., Bij de Vaate et al., 2021; Müller et al., 2014; St-Laurent et al., 2008), ocean stratification (e.g., Müller, 2012; Müller et al., 2014), and sea level rise (e.g., Devlin et al., 2017; Ross et al., 2017). Modeling studies suggest that climate change will continue to affect tides for centuries (Pickering et al., 2017; Schindelegger et al., 2018). Nevertheless, Haigh et al. (2020) indicated the need for better understanding of individual contributions of small-scale and large-scale processes.

An increasing number of studies are devoted to mapping and understanding secular changes in the tides. However, most of these studies rely on sea level observations from tide gauges that are mainly restricted to coastal and shelf regions. Hence, observed changes in tides could be dominated by local processes and the large-scale patterns remain unclear. Obtaining the global picture of long-term changes in tides would contribute to a better understanding of the drivers behind secular changes in tides. Understanding secular changes in tides may result in better identification and prediction of any consequences for coastal environments such as flooding (Li et al., 2021), salt intrusion (Hinton, 2000), or altered estuarine dynamics (Khojasteh et al., 2021).

To gain more insight in the large-scale secular changes in tides, we supplemented the clustered and sparsely distributed tide gauge dataset with data from satellite radar altimeters. Altimeter-derived water levels are being widely used to estimate tidal constants, and have recently been used to study seasonal changes in tides (Bij de Vaate et al., 2021; Müller et al., 2014). However, up to now, only Ray (2016) used altimeter data from successive missions to compare the amplitude of the main semi-diurnal tide (M_2) near Churchill, Hudson Bay (Canada). Given the length of the current satellite altimeter records (>25 years), from a theoretical point of view it should be possible to obtain estimates of the secular changes in tides from these data. For that reason, we have exploited the provided opportunities and used data from TOPEX/Poseidon and the Jason satellites to obtain a global estimate of the linear secular trends in the major tides. In this paper we first describe the data, including satellite radar altimetry, high-frequency tide gauge records and reanalysis data used for validation of the results. Then an outline is given of two approaches to study secular changes in tides and an experiment to test these methods. Finally, the results are introduced and compared to observations at tide gauges and documented changes in tides.

2. Data

2.1. Satellite Radar Altimetry

Data from the TOPEX/Poseidon and Jason satellite altimeters were combined (further referred to as TPJ) resulting in 28 years of sea level data (1993–2020). Data from interleaved orbits were not considered. The TPJ satellites have a ground coverage up to 66°N/S and an along-track resolution of about 5.8 km. Altimeter data were obtained through the Radar Altimeter Data System (RADS, Naeije, 2020). The following geophysical and range corrections were applied (Scharroo et al., 2016): ionosphere (NIC09 for TOPEX/Poseidon, GIM for Jason), dry troposphere (ECMWF), wet troposphere (if available: radiometer, otherwise: ECMWF), solid tide (Cartwright & Edden, 1973; Cartwright & Taylor, 1971), pole tide (Wahr, 1985), load tide (FES2014), mean sea surface (DTU18-MSS), sea state bias (CLS), and dynamic atmosphere (DAC) (MOG2d (ERA Interim forcing)). The center-of-gravity (CG) correction that the RADS by default applies to TOPEX/Poseidon ranges was removed to reduce intermission biases in the solar S_2 tide (Beckley et al., 2021; Zawadzki et al., 2018). In addition, to minimize aliasing of non-tidal sea level variability on tidal frequencies, an additional correction was applied. Following Ray and Zaron (2016), the multi-mission, gridded sea level anomalies (SLA) from the Data Unification and Altimeter Combination System (DUACS) (Mercator Ocean International, 2021; Taburet et al., 2019) were subtracted from the TPJ-water levels. This removes seasonal and interannual variability from the obtained water levels and specifically reduces the noise in regions with high mesoscale activity. In the remainder of the paper, this correction will be referred to as the 'mesoscale correction'. Finally, outliers in the time series were detected and removed based on three times the median absolute deviation.

In this paper, results are presented on global maps, supplemented by a zoom in on the North West European Shelf. For the global analysis, data are treated as follows. First, the locations where two tracks intersect (crossovers) were identified. For all of those locations, the data of the two crossing tracks within a radius of 30 km were assigned to the location of the respective crossover. The 30 km equals half the distance between the closest neighboring crossovers. Note that the along-track distance between crossovers depends on latitude: from ∼460 km at the equator to ∼60 km at 66° N/S. By stacking the data at crossover locations, the temporal resolution is increased and tidal analysis is deemed more reliable. For the zoom in on the North West European Shelf, data were processed on a track-by-track basis. Data from different cycles were collocated following Cherniawsky et al. (2010). The along-track analysis allows for a higher spatial resolution and to get closer to the tide gauge locations, at the price of an increase in uncertainty levels.

2.2. Tide Gauges

Alongside the altimeter data, data from a selection of tide gauges were processed to allow for a comparison of the derived trends. For this purpose, only tide gauge data from the TPJ-period were considered (1993–2020). Data from the GESLA-3 dataset (Haigh et al., 2021) were complemented with quality controlled water level records from tide gauges on the North West European Shelf, provided by nine European organizations (see Acknowledgments). The latter comprise data from 1997 onward, and are manually inspected to exclude possible outliers. Records that span less than 19 years were excluded. The temporal resolution of the tide gauge data varies from 1 minute to 1 hour, mainly depending on the country where the stations are located and the time of data

acquisition. Tide gauge records were corrected for atmospheric loading using the same product as was used for altimetry (DAC).

2.3. Reanalysis Data

Finally, reanalysis data were used to obtain uncertainty estimates of the estimated linear change in tidal constants. For this, the Global Tides and Surge Model (GTSM, Wang et al., 2021) was used, forced by ERA5 reanalysis data. GTSM is a barotropic (2D) model that makes use of an unstructured grid with a resolution that increases from 25 km at open ocean to 2.5 km at the coast. Time series with a sampling rate of 10 min were reconstructed for the full TPJ-period. This was done for over 600 locations covering the global oceans and about 300 locations on the western North West European Shelf. Subsequently, the time series were corrected for atmospheric loading (using the DAC), temporarily detided and then subjected to a high-pass filter to remove any non-tidal signal with periods larger than 2 days. This was done to mimic the 'mesoscale correction' that was applied to the TPJ-data. Although the GTSM does not resolve ocean circulation and associated mesoscale sea level variability, atmospheric forcing may induce seasonal/interannual sea level variability (e.g., Dangendorf et al., 2014), which is to some extent also contained in the 'mesoscale correction'.

3. Methods

Earlier studies on secular changes in tides typically relied on year-by-year harmonic analyses of high-frequency data, followed by the fitting of a linear trend through the yearly tidal harmonic constants (e.g., Müller et al., 2011; Ray, 2009; Zaron & Jay, 2014). In this paper, a similar procedure was adopted to process the tide gauge data. However, for satellite data, such a procedure is not possible due to the relatively low sampling rate and consequent aliasing of high-frequency tidal signals onto lower frequencies. That is, for the major tides, the TPJ-sampling interval of 9.9156 days results in alias periods of 62.1 (M_2), 58.7 (S_2), 173.2 (K_1), and 45.7 days (O_1) (Cherniawsky et al., 2010; Schrama & Ray, 1994). By applying the Rayleigh criterion to these alias frequencies, we can find the minimum record length that is required to separate the tides of interest from other signals (Savcenko & Bosch, 2007). For M_2, S_2, and O_1, records of three (2.97) years are sufficient to separate them from other considered constituents, while at least 9.19 years are required to separate K_1 from S_{sa} (semi-annual tide). Hence, a year-by-year harmonic analysis of TPJ-data is not possible. In this paper, two different methods were implemented.

Both approaches make use of UTide (Codiga, 2020). This software executes a harmonic analysis for a given set of frequencies similar as in TTide (Pawlowicz et al., 2002), yet it is able to deal with irregular temporal sampling. The latter is a requirement for processing stacked altimeter-derived water levels. For the analysis of tide gauge data, a large set of constituents (including shallow water constituents) was considered following from the automated constituent selection method in UTide (Codiga, 2020; Foreman, 2004). For satellite data, a fixed set of constituents was considered, as explained below.

3.1. Segmented Harmonic Analysis

The first approach, referred to as the 'segmented harmonic analysis' (SegHA) approach (inspired by Jin et al. (2018)), is a two-step procedure that is very similar to the conventional analysis of secular changes using tide gauge data. This approach could be carried out with standard tidal analysis tools, but comes at the price of a slight simplification in error propagation.

3.1.1. Step 1: Estimation of Tidal Harmonic Constants

Instead of processing the data year-by-year, time series were split in seven consecutive periods of 4 years. Thereafter, tidal harmonic constants were calculated and referred to the center date of the respective 4-year period. The time span of 4 years was chosen primarily because this allows the separation of M_2, S_2, and O_1 from other signals (this requires at least 3 years). On the other hand, there is in some instances (mainly coastal) a discrepancy between the actual nodal modulation of lunar tides (18.6 years cycle) and the theoretical value (Hagen et al., 2021). Hence, although amplitude/phase estimates are corrected for the nodal modulation during tidal analysis, there may be a residual modulation left. To separate the trend in tidal amplitude from this possible residual nodal modulation, the difference between the respective center data of the first and last period was required to

be at least 18.6 years. This can be achieved by processing segments of up to 5 years (segments are not allowed to overlap). Hence it is anyway not possible to study the secular trend in K_1 harmonic constants from the available data using the SegHA approach. Given the minimum of 3 years and the maximum of 5 years, a time span of 4 years was chosen since this allows making full use of the available data (28 years).

For each 4-year period, tidal amplitudes and phases were estimated for 20 tidal constituents, including: three long-period tides (S_a, M_m, and M_{sf}), five diurnal tides (Q_1, O_1, P_1, S_1, and K_1), eight semi-diurnal tides ($2N_2$, μ_2, N_2, ν_2, M_2, L_2, T_2, S_2, and $2SM_2$), and four shorter period tides (M_3, MN_4, M_4, and MS_4). This selection of constituents eliminates possible conflicts between constituent's pairs that cannot be separated from 4 years of data (e.g., K_1 and S_{sa}). In addition, from each 4-year period the mean sea level (Z_0) and a possible trend in mean sea level were estimated to account for any remaining interannual sea level variability.

95% confidence intervals for the estimated harmonic constants were computed with UTide. This measure is derived from linearized error propagation of the total residual power (using the detided signal) within the frequency band surrounding the frequency in question ($M_2/S_2 \pm 0.2$ cycles/day and $O_1 \pm 0.1$ cycles/day), obtained using the Lomb-Scargle periodogram (Codiga, 2011; Pawlowicz et al., 2002). However, it is stated by Codiga (2011) that certain assumptions underlying this procedure are strictly valid only for uniformly sampled data. The resulting confidence intervals "should be considered potentially reasonable and approximate first estimates, but should be compared against the results for uniform times whenever possible, and used with a measure of caution." (Codiga, 2011, p. 21). Indeed, it was found that both the frequency and timing of the sea level measurements by the satellite influenced the accuracy of the resulting tidal estimates (Guarneri et al., 2022). Moreover, UTide averages the spectral density distribution of the residuals over nine frequency bands resulting in similar confidence intervals for all diurnal tides, all semi-diurnal tides, and so on. In line with the advice from Codiga (2011), but due to the lack of tide gauge data in the vicinity of the altimeter points, we have therefore obtained an additional (alternative) uncertainty estimate using the reanalysis data that were introduced in Section 2.3. These time series were reduced to a 4-year period (2015–2018) and interpolated to the TPJ-sampling interval of which the start time was iteratively shifted by about 4.75 hr (TPJ-sampling period divided by 50), resulting in 50 time-shifted time series. The median absolute deviation (MAD) of the tidal harmonic constants estimated from these 50 time series, was scaled by 1.4826 to obtain the standard error of the estimate (Rousseeuw & Croux, 1993). The final values are location- and tide specific, but assumed to be independent of the 4-year period.

3.1.2. Step 2: Linear Trend Estimation

The linear secular trends in harmonic constants were estimated by fitting the following equations through the series of seven values, using weighted least squares. Here the error propagation was simplified by ignoring the correlations between amplitudes and phases estimates. For amplitudes follows:

$$\tilde{A}_k(t_i) = \underbrace{a^A_{N_k} \cos\left(2\pi \frac{t_i - t_c}{18.6} + N_c\right)}_{\text{residual nodal modulation}} + \underbrace{b^A_k (t_i - t_c)}_{\text{trend}}. \quad (1)$$

where, $\tilde{A}_k(t_i)$ is the residual amplitude for the ith 4-year period of the tidal constituent in question (k) (obtained by subtracting the time averaged amplitude), b^A_k the linear change in amplitude, t_i the center time of the ith 4-year periods, and t_c the center time of the full TPJ-period. In addition, the nodal modulation was included in the problem formulation (see Section 3.1.1). N_c represents the nodal phase at the center date. Both the magnitude of the residual nodal modulation $\left(a^A_{N_k}\right)$, and the linear amplitude change $\left(b^A_k\right)$ were estimated, resulting in a redundancy of five. For the phases the following equation was used:

$$\tilde{\phi}_k(t_i) = \underbrace{a^\phi_{N_k} \cos\left(2\pi \frac{t_i - t_c}{18.6} + N_c\right)}_{\text{residual nodal modulation}} + \underbrace{b^\phi_k (t_i - t_c)}_{\text{trend}}. \quad (2)$$

where $\tilde{\phi}_k(t_i)$ is the residual phase for the ith 4-year period, $a^\phi_{N_k}$ the magnitude of the residual nodal phase modulation, and b^ϕ_k the linear coefficient describing the change in phase.

Both the standard errors of the harmonic constants derived from UTide and from GTSM (Section 3.1.1) were used to assess the significance of the fitted trends. For the S_2 tide, the choice of ionospheric correction applied to the data may affect the estimated tidal harmonic constants (Jee et al., 2010; Ray, 2020; Zawadzki et al., 2018).

Therefore, an additional error estimate was obtained (see Text S1 in Supporting Information S1) and added to the estimates obtained by UTide and GTSM, respectively. Given the standard errors of the tidal harmonic constants, the standard error of the trend was derived through error propagation. Finally, confidence intervals were obtained by multiplying the standard error with the appropriate z-score.

3.2. Trend-Integrated Harmonic Analysis (TintHA)

In the second approach, the linear trends in the four tides of interest (M_2, S_2, O_1, and K_1) were estimated jointly with the average tidal harmonic constants. This required an extension of the available tidal analysis software but allowed for a full error propagation (i.e., including the co-variances between amplitude and phase estimates). Since we are now using the full 28 years of data, this approach allows the analysis of changes in the K_1 tide. Moreover, the set of constituents included in the analysis was extended by S_{SA}, K_2, and T_2. In the SegHA approach, these had to be excluded due to aliasing issues.

The TintHA approach uses a different formulation of the tides. Within UTide, the complex formulation is used in which the tidal water level for constituent k, that is, $\hat{h}_k(t)$, is written as the product of three terms:

$$\hat{h}_k(t) = \left(A_k e^{i\phi_k}\right)\left(f_k(t)e^{iu_k(t)}\right)e^{iv_k(t)}, \tag{3}$$

where the term $e^{iv_k(t)}$ is the phase of the equilibrium tide, $\left(f_k(t)e^{iu_k(t)}\right)$ is the nodal correction, and the term $\left(A_k e^{i\phi_k}\right)$ is the complex amplitude-phase pair that needs to be estimated. To keep the equations linear, we consider the complex amplitude-phase pair $\hat{A}_k = A_k e^{i\phi_k}$:

$$\hat{A}_k(t) = \hat{F}_k + \hat{G}_k \frac{t - t_0}{T}, \tag{4}$$

where the time period considered starts at t_0 and ends at $t_0 + T$, so that $\hat{A}_k(t_0) = \hat{F}_k$ and $\hat{A}_k(t_0 + T) = \hat{F}_k + \hat{G}_k$. The relative change over this time period is $\hat{\Delta} = \left(\hat{F}_k + \hat{G}_k\right)/\hat{F}_k$. The angle and absolute value of this complex number give the phase change and relative amplitude change. A disadvantage of this linear model is that the rate of change of the amplitude and phase is not constant over the time interval. For small changes, however, the approximation error will be small. Note that in this method no empirically estimated correction for any residual of the nodal modulation is determined as this, in combination with the trend estimation, would result in a non-linear estimation problem.

Similar to the first approach (SegHA), alternative error estimates were obtained by means of the GTSM reanalysis data. For the latter, the full 28 years time series were interpolated to TPJ-sampling intervals while iteratively shifting the start time 50 times. From these time series the linear change in tidal harmonic constants was computed and the MAD of these values was again scaled by 1.4826 to obtain the standard error of the trend estimates. For the S_2 tide, the error estimates were supplemented by the possibly error due to the ionospheric correction (as described in Text S1 in Supporting Information S1). Finally, the confidence intervals were obtained by multiplying the error estimate by the appropriate z-score and interpolating the GTSM-derived product to the TPJ-tracks.

3.3. Validation

3.3.1. Comparison of SegHA and TintHA Using Tide Gauge Data

Both methods (SegHA and TintHA) were assessed by application to tide gauge data that were sub-sampled to TPJ-sampling intervals. This was done in a similar manner as the GTSM reanalysis data were used to compute confidence intervals. Data were subsampled both to an along-track sampling of 9.9156 days and a crossover sampling which was determined based on the TPJ crossover sampling at the latitude of the respective tide gauge. The start time of the subsampled time series was iteratively shifted, resulting in 50 time series for each tide gauge. For the assessment, only tide gauges were considered that have full data coverage during the entire TPJ-period. In addition to DAC, the 'mesoscale correction' was applied to the data to resemble the processing of altimeter data. As this altimetry-derived product is not available everywhere across the globe, only the data from 109 tide gauges could be used. The secular change in tidal harmonic constants derived from both methods was compared to the 'true' change that was obtained by processing the original high-frequency data on a year-by-year basis. Assessment of the different methods was done by comparing the median absolute error (MedAE) for respectively each tide gauge, tidal constituent and sampling scheme.

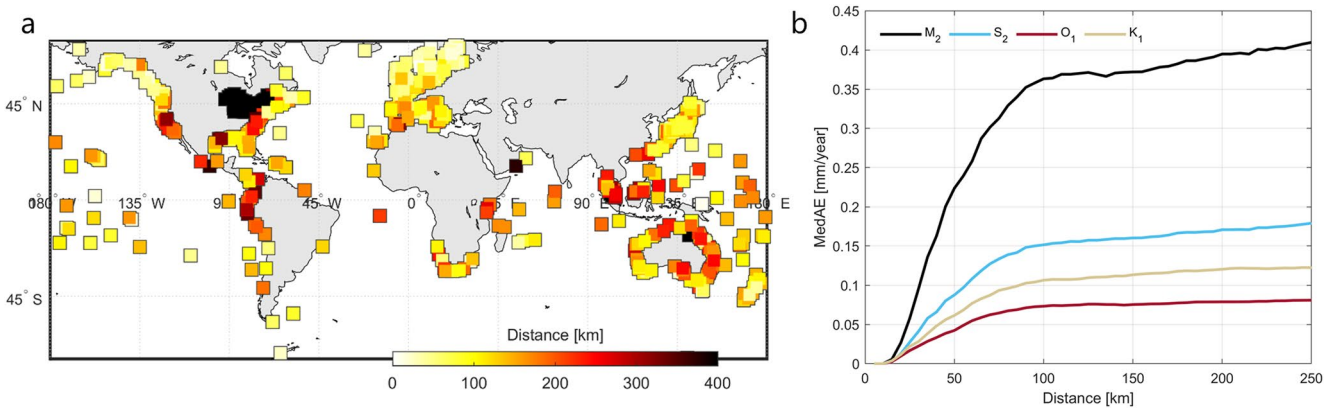

Figure 1. Distance between each tide gauge and the nearest TPJ-crossover (a). Spatial error (MedAE) in estimated secular trends in tidal amplitude as a function of distance, derived from the tide gauge data (b).

3.3.2. Comparison of Confidence Intervals Using Tide Gauge Data

As discussed in Section 3.1.1, two alternative confidence intervals were obtained for the trend estimates: one following from UTide, the other from processing of GTSM reanalysis data. To validate both alternatives, an additional experiment was performed using the results from the experiment with tide gauge data (Section 3.3.1). This time, the scaled MAD of the trend estimates from the TPJ-sampled tide gauge data was used to compute 95% confidence intervals. These were then compared to the 95% confidence intervals obtained from UTide (based on the TPJ-sampled tide gauge data) and those derived using GTSM reanalysis data from the exact location as the tide gauges. This was done for both the regular along-track, as well as the latitude dependent crossover sampling. Results were analyzed based on the correlation, the root-mean-square error (RMSE), and the median underestimation of respectively the GTSM/UTide product.

3.3.3. Validation of Estimated Secular Change Using Tide Gauge Data

In order to validate the secular changes derived from TPJ-data by means of another product, ideally the data needs to be from the exact same location. Since this data is not available, we need to consider the impact of the spatial separation on the consistency of estimated secular change. As can be seen in Figure 1a, the distance between the tide gauges and the nearest TPJ-crossover varies from approximately 50 km to over 400 km. In addition, Figure 1b shows that the spatial error (MedAE) in estimated amplitude change (comparing every individual tide gauge to other tide gauges within a certain radius) increases with distance. Based on this figure, it was decided to only use tide gauges that are closer than 75 km to one or more TPJ-crossovers (indicated by the thicker outlines in Figures 7 and 8) for the assessment of agreement between tide gauges and TPJ-data. From the 176 remaining tide gauge-crossover combinations, the absolute differences in estimated trend were computed. The differences were then classified as being insignificant for combinations where the confidence interval of the trend estimate at the crossover (as derived from GTSM, see Figure 6b) exceeded the difference.

3.4. Post-Processing

Estimated trends were omitted for locations where at least one of the following criteria was not met. If not mentioned otherwise, these criteria were applied in the analysis of the crossovers, individual tracks, and tide gauges:

- The root-mean-square (RMS) of the residual signal should be below 0.15 m. Globally, this removes ~8% of the data.
- There should be consistent data coverage throughout the year. A location was not considered when there are more than 10 sequential day numbers without data. Globally, this removes ~20% of the data.
- The estimated linear coefficient should be larger than its confidence interval. Which confidence intervals were used is mentioned in figure captions.
- Only applied in a long-track analysis: crossovers where there is no overlap between the estimated linear trends of the two crossing tracks (interpolated to the location of the crossover) ± the local confidence interval, were flagged. In such a case, all derived trends of the two crossing tracks within half the distance between neighboring crossovers were omitted.

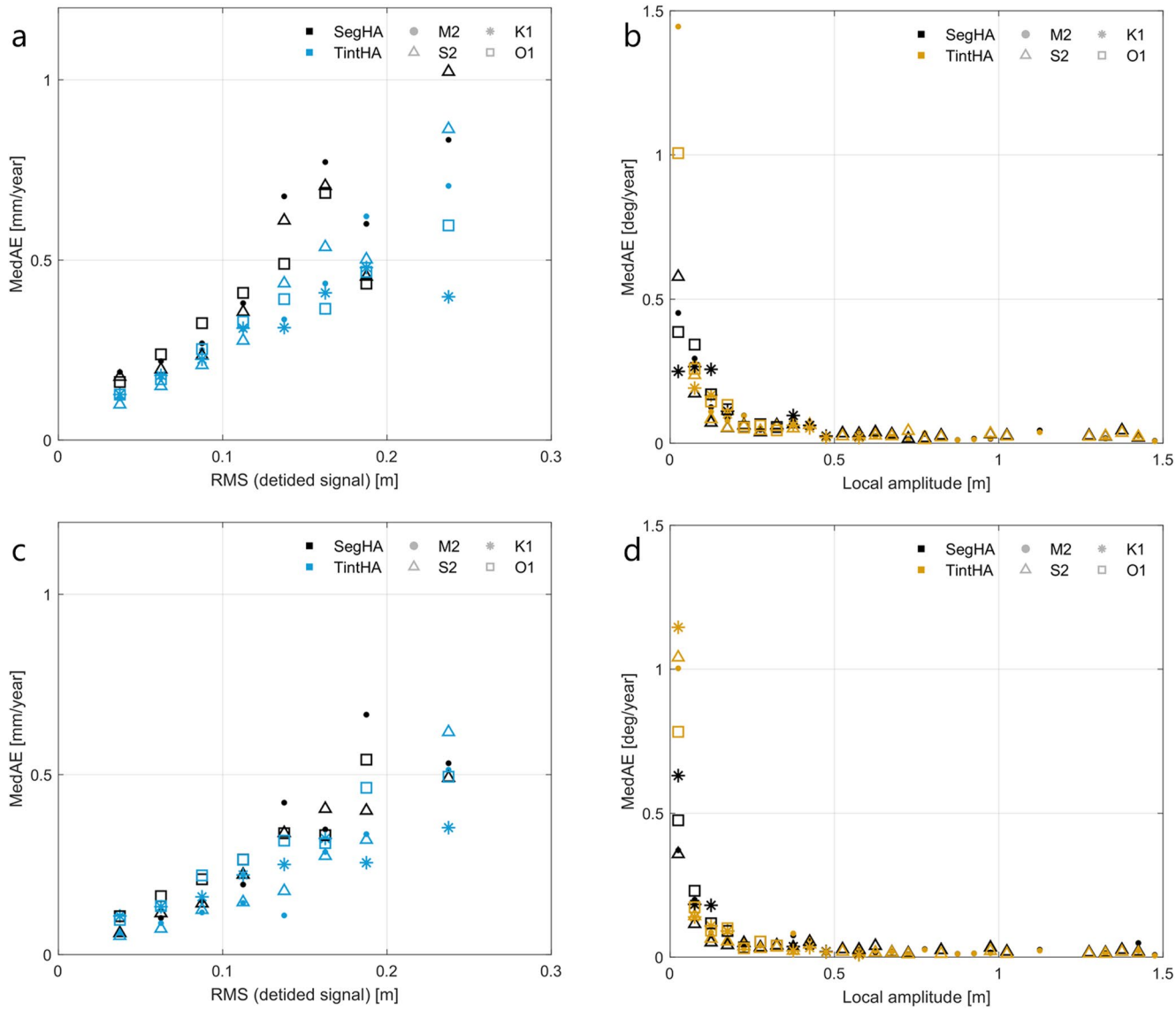

Figure 2. Median absolute error (MedAE) between the 'true' linear change in amplitudes (a), (c) and phases (b), (d) derived from high-frequency tide gauge records and the product derived from the SegHA and TintHA approaches applied to the data sub-sampled at TPJ along-track sampling intervals (a), (b) and TPJ crossover sampling (c), (d). Colors indicate which method was used and the marker style depicts the different tidal constituents that were studied. For visualization purposes the errors are averaged for intervals of 0.025 and 0.05 m for the RMS (detided signal) and local amplitude respectively.

4. Results

4.1. Validation

4.1.1. Comparison of SegHA and TintHA Using Tide Gauge Data

Comparison of both methods applied to tide gauge data shows little difference between the SegHA and TintHA methods (Figure 2). Regardless of the method that was used, sub-sampling the data to TPJ-sampling interval reduces the accuracy of the derived changes in tidal amplitude and phase. In the case of amplitude, the observed error between the 'true' and derived change increases with larger non-tidal water level variation (higher RMS; Figure 2a). On the other hand, the accuracy of the derived phase change predominantly depends on the local amplitude of the tide in question (Figure 2b). In particular for amplitudes below ~15 cm, the derived phase change appears unreliable. Only in terms of amplitude change, the TintHA method performs more consistent than the SegHA method, with an average MedAE of 0.24 mm/year compared to 0.29 mm/year and fewer outliers.

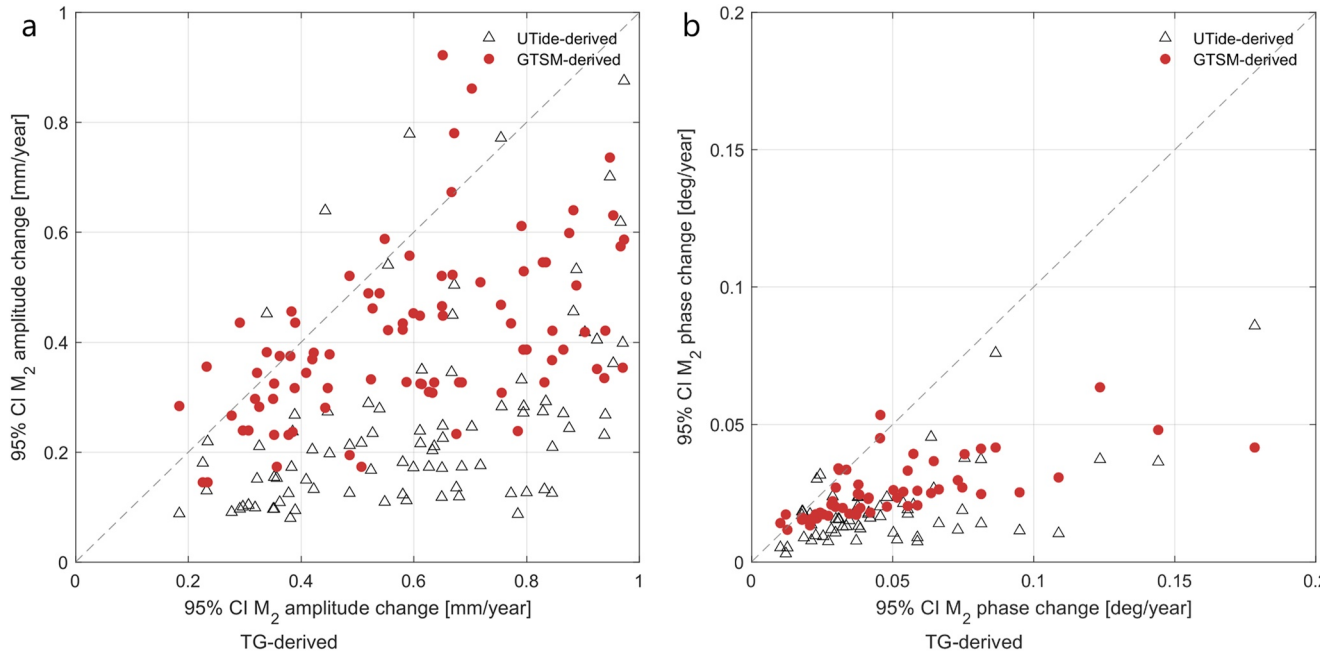

Figure 3. 95% confidence intervals derived from UTide, GTSM reanalysis data and the tide gauges as described in Section 3.3.2 for the change in M_2 amplitude (a) and phase (b), following from the TintHA approach and along-track sampling.

Overall, the crossover sampling improves the accuracy of both methods for both amplitudes (MedAE reduces from 0.25 mm/year to 0.18 mm/year) and phases (0.18°/year to 0.13°/year) for all tides (Figures 2c and 2d).

4.1.2. Comparison of Confidence Intervals Using Tide Gauge Data

The UTide-, GTSM- and tide gauge derived confidence intervals for the change in M_2 amplitude (a) and phase (b) are shown in Figure 3, following from the TintHA approach. From the figure, it appears that both the UTide and the GTSM-product subceed the confidence intervals derived from the tide gauges (i.e., more scatter points are located in the bottom right). However, statistical analysis of the results (all tides combined) show that the tide gauge derived confidence intervals correlate better with the GTSM product (correlation of 0.62 for amplitude, 0.67 for phase) than with the UTide product (amplitude: 0.53, phase: 0.55). In addition, the RMSE is lower for GTSM (0.37 mm/year and 0.05 deg/year) than for UTide (0.46 mm/year and 0.08 deg/year). In terms of underestimation of the confidence intervals for amplitude change, the GTSM product again performs better than UTide (0.15 mm/year vs. 0.26 mm/year). Concerning the phase changes, the GTSM product performs slightly better (0.02 deg/year vs. 0.03 deg/year). However, note that the phase results for O_1 and K_1 are based on only 11/12 tide gauges (compared to 61 and 53 for M_2 and S_2, respectively). Tide gauges where the tidal amplitude was below 15 cm were excluded, because a low tidal amplitude increases the uncertainty of phase change estimates to such an extent that any differences between the different confidence interval products become irrelevant (also shown by Figures 2b and 2d). However as these differences were typically large, they would dominate the statistics and overshadow the results that do matter.

Moreover, it was found that while the tide gauge and GTSM-derived confidence intervals are significantly lower for the crossover sampling than for the along-track sampling (respectively 25% and 27% for amplitude, 27% and 17% for phase), the UTide confidence intervals were less affected (4% for amplitude 6% for phase).

4.2. Global Analysis

The estimated trends in amplitude at the TPJ-crossovers following from the TintHA approach, are displayed in Figures 4 and 5. The results produced by the SegHA method are very similar and incorporated in the Supporting Information (Figure S6 in Supporting Information S1). Clearly, regions that are covered by sea ice during part of the year (above 55° N/S), have insufficient data availability for this analysis and are excluded. The distribution of locations where the estimated trend coefficients are significant, varies per tidal constituent, which is closely

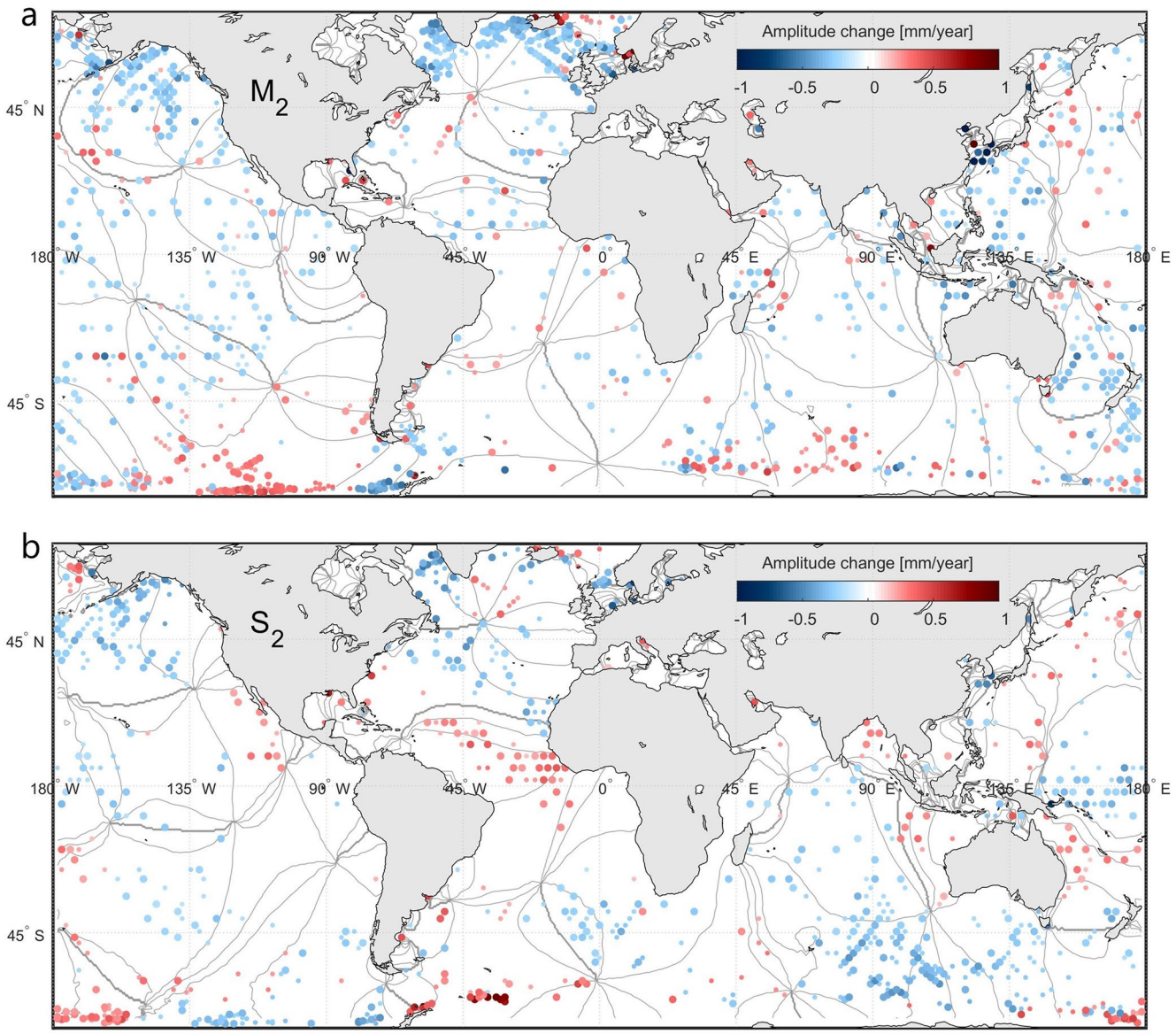

Figure 4. Linear change in M_2 (a) and S_2 amplitude (b) per year (1993–2020) following the TintHA approach. Locations where the post-processing criteria were not met are excluded from the figure. The smaller scatters indicate data that exceeds both the UTide and GTSM 90% confidence intervals, while the larger scatters indicate significant data at the 95% confidence level. Lines in the background depict tidal phases at 45° intervals.

related to the confidence intervals (Figure 6 and Figures S2 and S3 in Supporting Information S1). In most cases, the GTSM-derived confidence intervals (e.g., Figure 6b) exceed the intervals derived by UTide (Figure 6a).

As can be seen in Figures 4 and 5, all tides are subject to yearly changes of up to ±1 mm/year. The magnitude and sign of the yearly change vary largely across the globe, while the spatial correlations of the signal vary per tide. For M_2, the change in amplitude is predominantly negative. The most obvious regions of positive change are in the south, near Antarctica and east of Iceland (Figure 4a). Although the overall change is rather heterogeneous, spatial correlation of the signal is stronger near the poles than at the lower latitudes. On the contrary, the change in S_2 amplitude shows more distinct regions of either positive or negative change across the globe (Figure 4b). Predominantly positive changes in amplitudes are observed around the equator and near the poles, while negative changes are more restricted to mid-latitudes. Differences in sign of the amplitude change appear closely related to the location of amphidromic points and co-phase lines. The change in O_1 amplitude is more similar to that of M_2, concerning the level of heterogeneity (Figure 5a). However, overall, the change in O_1 amplitude is a lot smaller

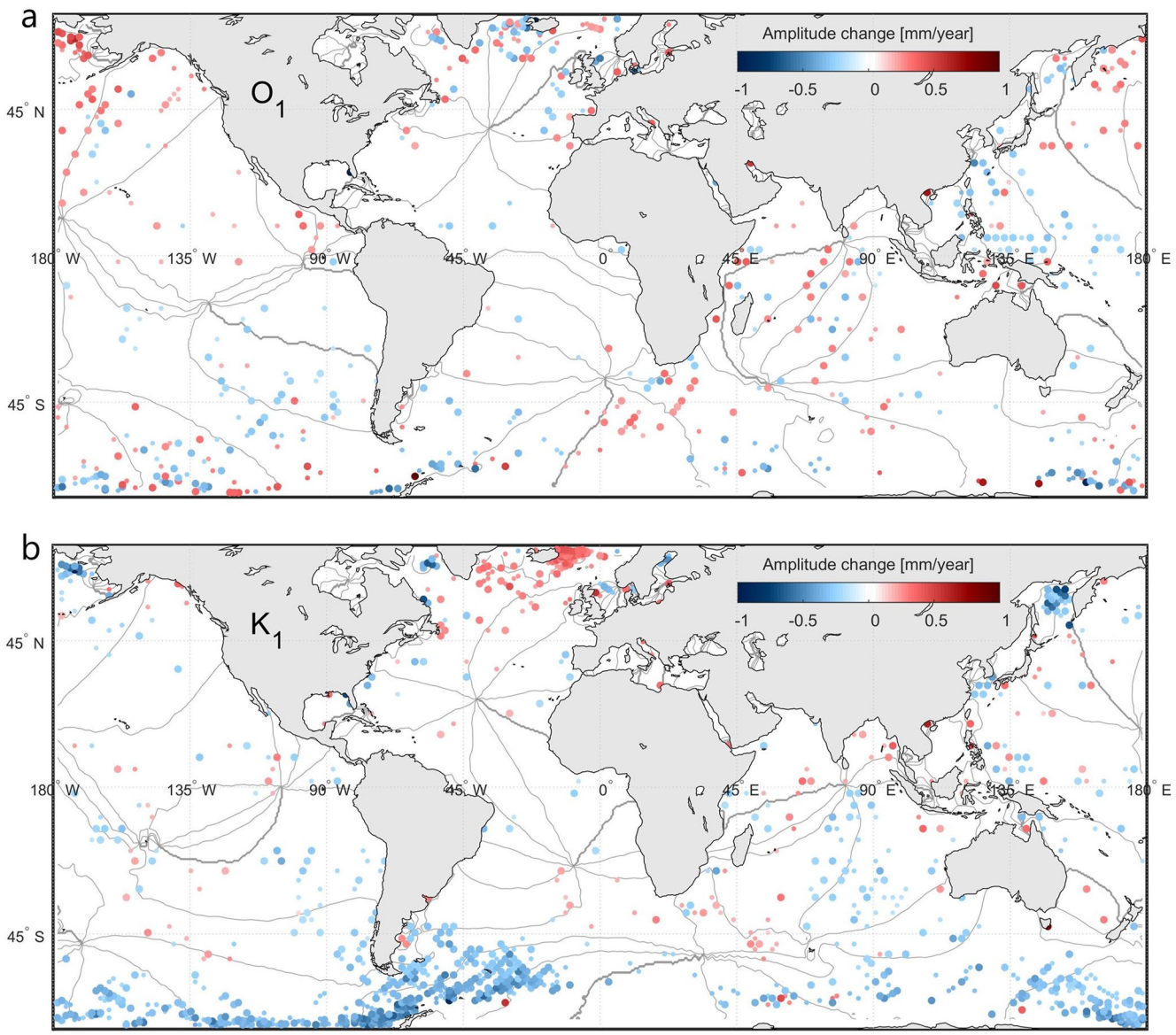

Figure 5. Linear change in O_1 (a) and K_1 amplitude (b) per year (1993–2020) following the TintHA approach. Locations where the post-processing criteria were not met are excluded from the figure. The smaller scatters indicate data that exceeds both the UTide and GTSM 90% confidence intervals, while the larger scatters indicate significant data at the 95% confidence level. Lines in the background depict tidal phases at 45° intervals.

than that of M_2 and only in a few locations, the confidence intervals are exceeded. For K_1, predominant negative changes are observed across the globe, except for the north Atlantic and the Indian Ocean (Figure 5b).

Trend estimates derived from the global tide gauge dataset are shown in Figures 7 and 8. For M_2, 41% of the differences in trend estimates from tide gauges and TPJ-crossovers were statistically insignificant considering the 95% confidence intervals derived from GTSM. For S_2 this value was 59%, for O_1 64% and for K_1 59%. However, note that in Figure 1b we observed a significant decrease in consistency among tide-gauge derived estimates with increased distances among the tide gauges. Given the fact that the distance between TPJ-crossovers and most tide gauges is at least 50 km, this explains part of the inconsistency between the altimeter- and tide gauge derived estimates. This in particular applies to M_2.

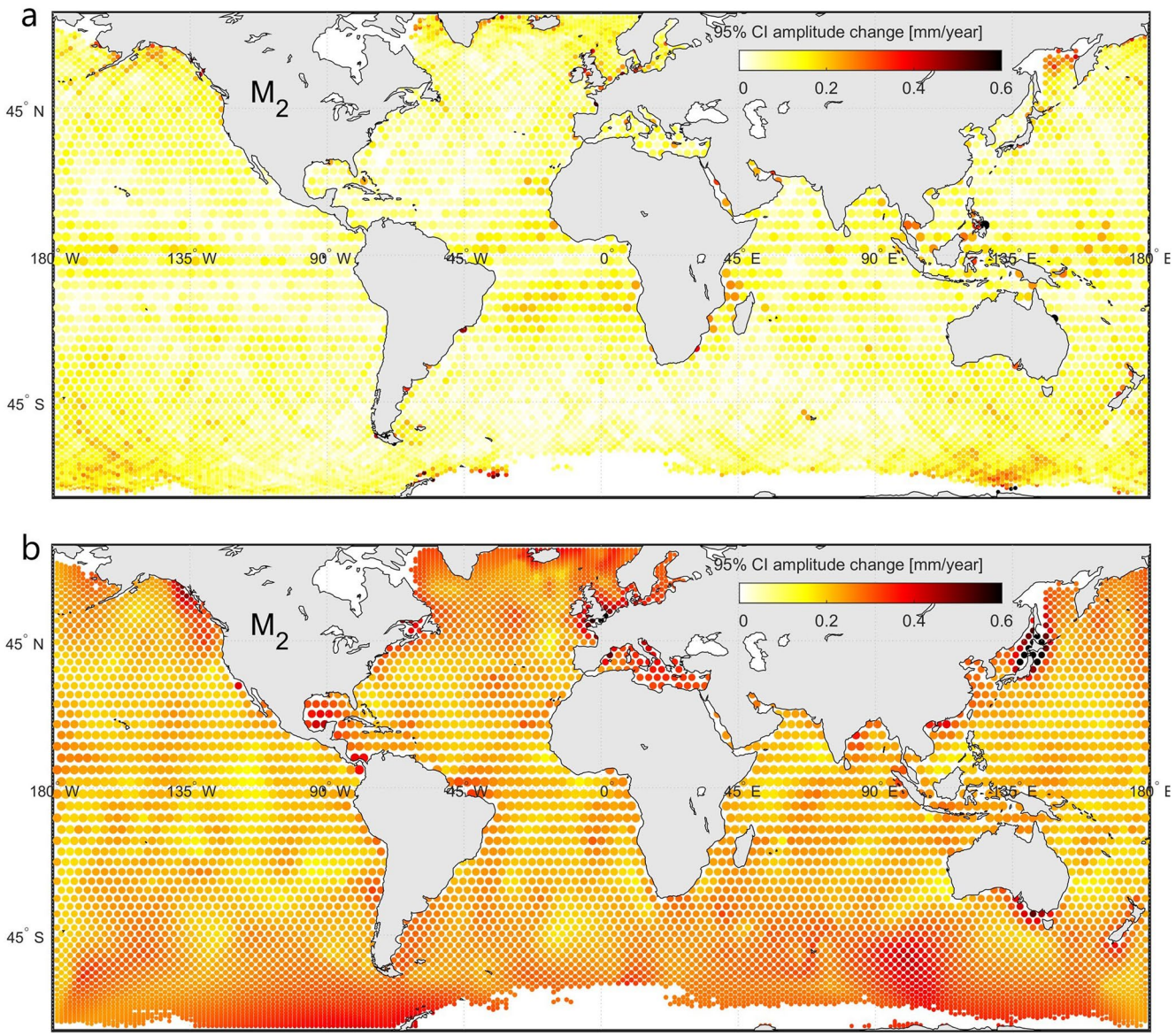

Figure 6. 95% confidence intervals for trend estimates derived from confidence intervals computed by UTide (a) and from standard errors derived from GTSM (b) for M_2 amplitude.

4.3. North West European Shelf

A selection of results from the along-track analysis of the North West European Shelf region is displayed in Figure 9. Because of their relatively low amplitudes in the region (<0.15 m), O_1 and K_1 are not included here.

The M_2 amplitude change derived from altimetry is predominantly negative across the domain, except for the central North Sea and the Skagerrak (Figure 9a). The largest change is observed toward the eastern coasts of the North Sea. Unfortunately most of the tide gauges are located along the coastline while RADS does not include coastal altimeter data. Nevertheless, the observed amplitude change at the tide gauges in the Netherlands, Germany, Denmark (and to a smaller extent the United Kingdom and Norway), is similar to that at nearby tracks. Limited similarity is observed for the tide gauges in the English Channel, the Irish sea and on the west coast of Norway. The altimetry-derived change in M_2 phase is largest near the amphidromic points in the North Sea and in the northwest corner of the region (Figure 9c). Overall, both the sign of the phase change as derived from altimetry as well as from tide gauges, is highly variable within the domain. In addition, the availability of significant

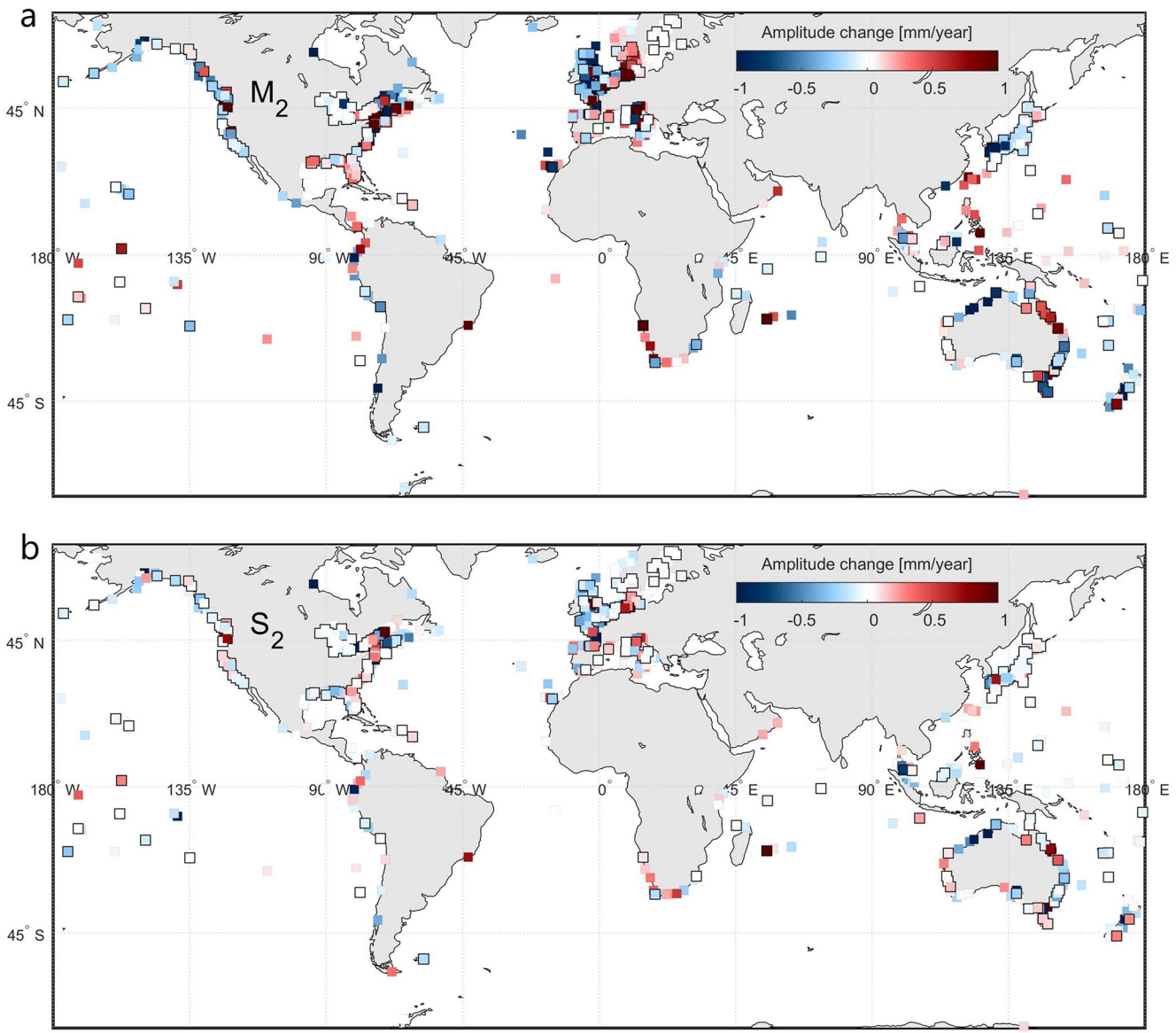

Figure 7. Secular trends in M_2 (a) and S_2 (b) amplitudes, derived from tide gauge records from the TPJ-period (1993–2020) (from GESLA-3; Haigh et al., 2021). Black-outlined tide gauge locations are within 75 km of a TPJ-crossover and are used for the similarity measure as explained in Text S2 in Supporting Information S1.

altimetry-derived phase changes near tide gauges is even more limited than was the case for the amplitude, making a comparison difficult.

The observed trends in S_2 amplitude are smaller than those in M_2 amplitude (Figure 9b), while the change in phase is larger (Figure 9d). These differences in magnitude are also observed at the tide gauges. However, tide-gauge and altimeter-derived estimates for S_2 agree in only few locations, predominantly along the Dutch coastline.

Both the GTSM and UTide-derived confidence intervals increase towards the coast for the amplitude change (Figures 10a, 10b and 11a and 11b) and towards amphidromic points for the phase change (Figures 10c, 10d and 11c and 11d). In all cases, the GTSM-derived confidence intervals exceed the ones computed by UTide. This is most noticeable for the S_2 amplitude change. Both GTSM- and UTide-derived confidence intervals for S_2 phase change are significantly larger than for M_2.

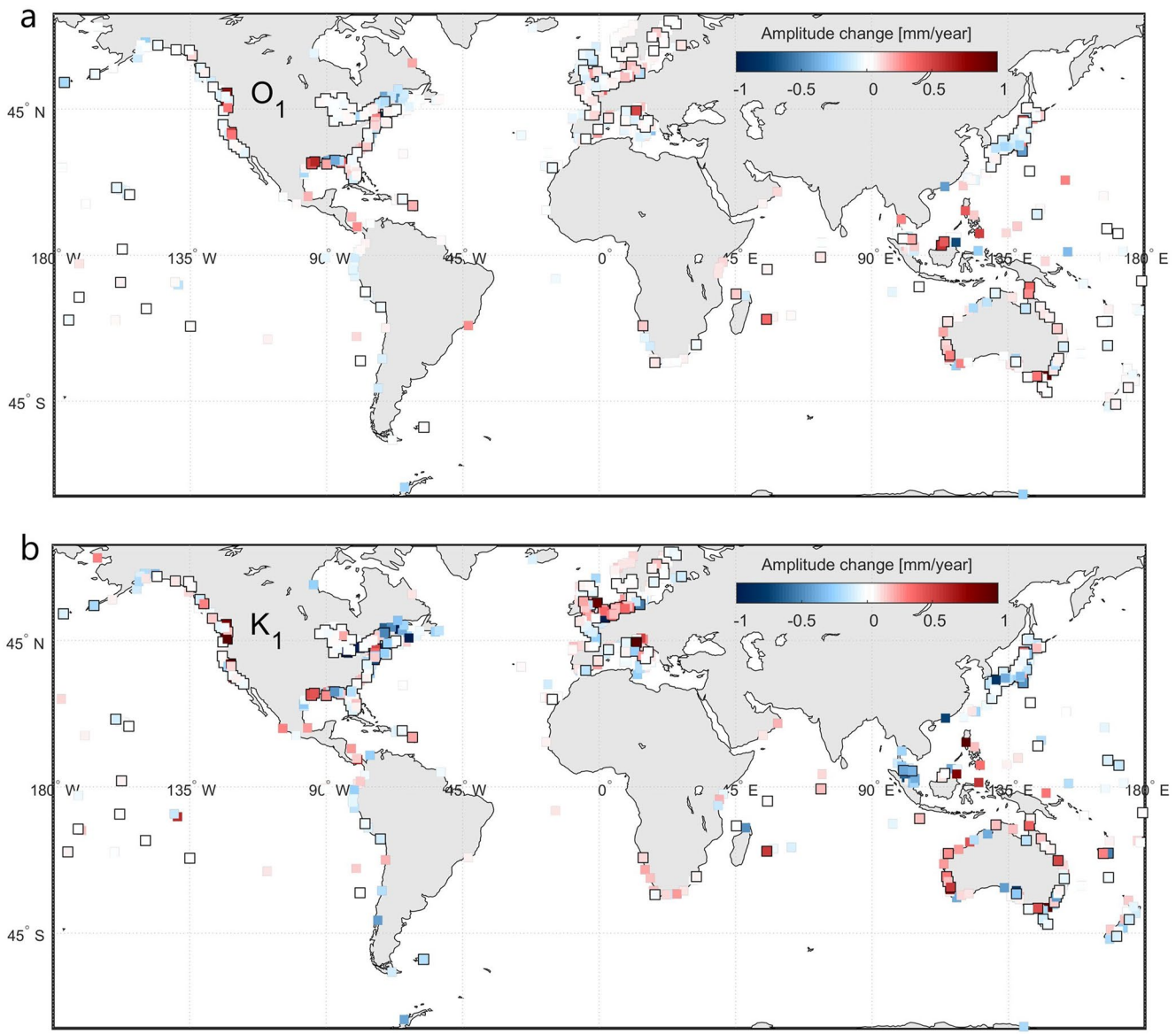

Figure 8. Secular trends in O_1 (a) and K_1 (b) amplitudes, derived from tide gauge records from the TPJ-period (1993–2020) (from GESLA-3; Haigh et al., 2021). Black-outlined tide gauge locations are within 75 km of a TPJ-crossover and are used for the similarity measure as explained in Text S2 in Supporting Information S1.

5. Discussion and Conclusions

Using the full record of sea level measurements by the TOPEX/Poseidon and Jason satellites (1993–2020), a global estimate of the secular trends in M_2, S_2, O_1, and K_1 tidal harmonic constants was obtained. While satellite altimetry is routinely used for tidal analyses, this is the first time it was used to study secular trends on a global scale. With this, the presented study attempts to fill in the gaps left by earlier studies on secular changes in tides, that were predominantly based on data from tide gauges. However, compared to tide gauges, the temporal resolution of the satellite data is limited. Consequently, several years of data were required to prevent aliasing and obtain reliable tidal estimates. Therefore, the method that is typically used to study secular changes in tides from tide gauge data, by means of yearly harmonic analysis, could not be applied. In this paper two alternative approaches were implemented. The first method (SegHA) is very similar to the yearly analysis except now the time series were divided into periods of 4 years. Compared to the yearly analysis, this reduces the number of consecutive independent tidal estimates and hence the redundancy in trend fitting and the significance of the estimated trends. Moreover, with this approach uncertainty estimates were obtained through a simplified error propagation

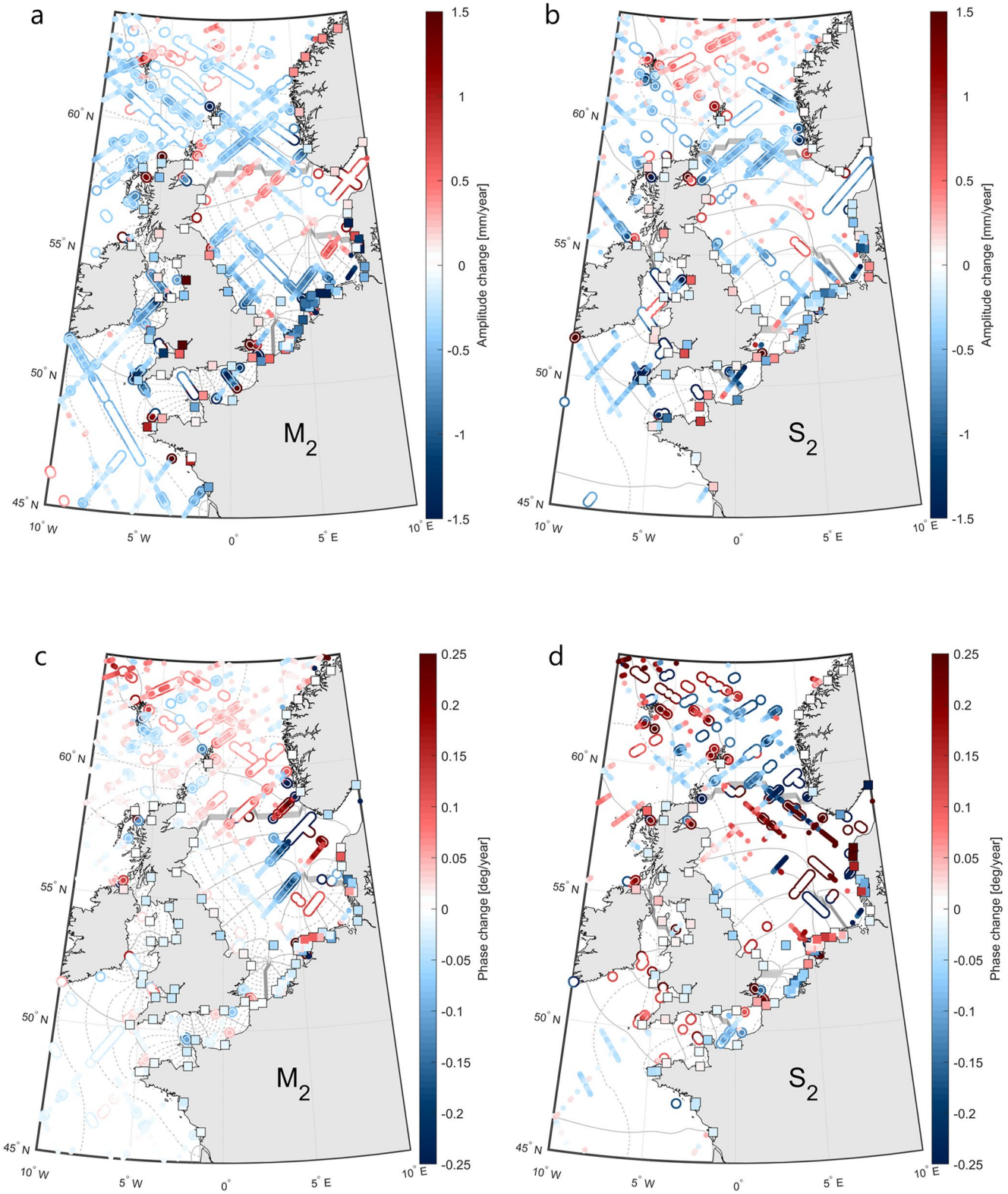

Figure 9. Linear change in M_2 amplitude (a), S_2 amplitude (b), M_2 phase (c) and S_2 phase (d) per year derived with the TintHA approach. The smaller solid scatters indicate significant trends given the UTide-derived 95% confidence intervals, the hollow outline indicates significance according to the GTSM-derived 95% confidence intervals (see Section 3). Co-tidal maps are shown in the background where the solid line indicates the phase at 45° intervals, the dashed lines show the amplitudes at 0.25 m intervals.

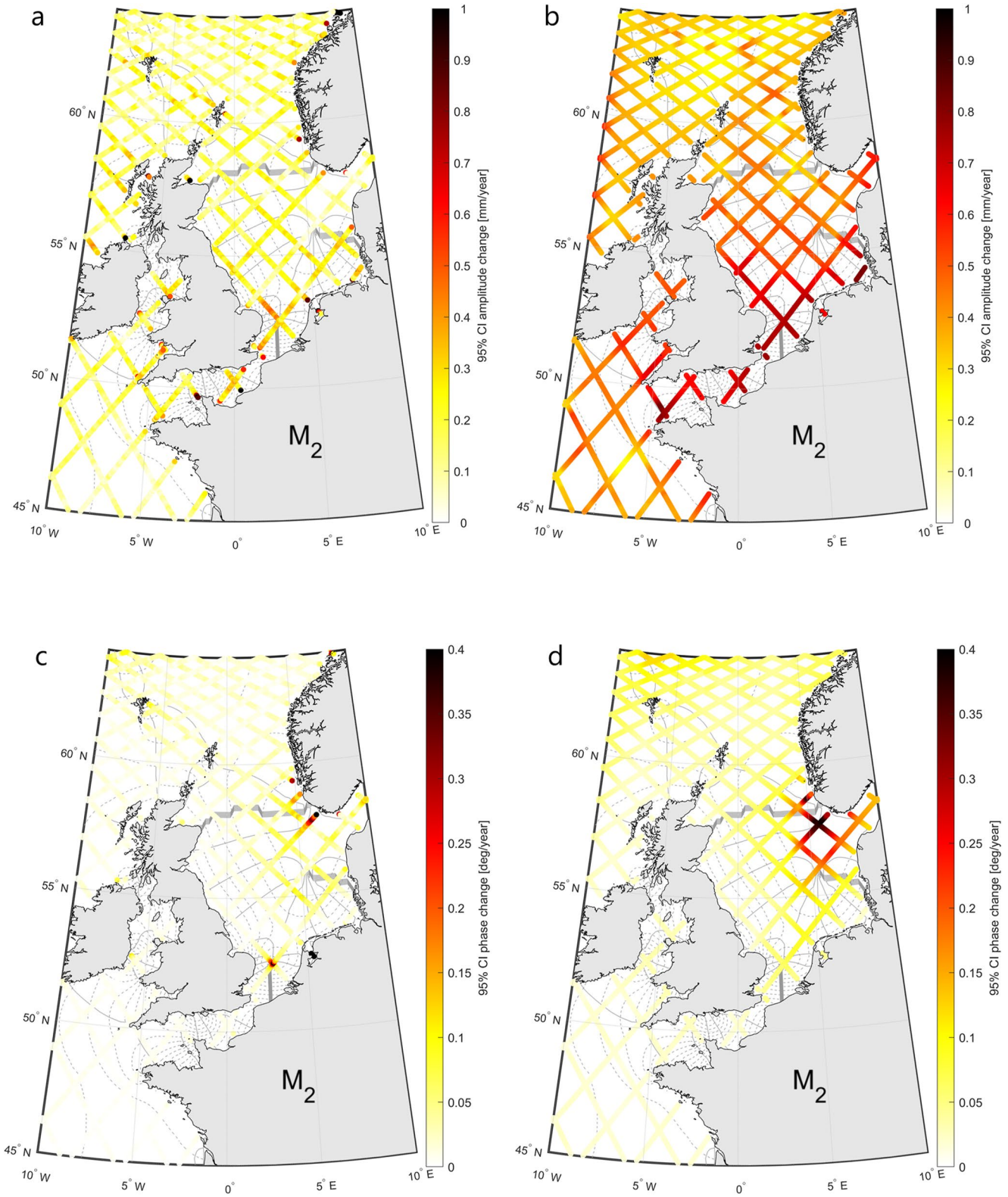

Figure 10. 95% confidence intervals for trend estimates derived from confidence intervals computed by UTide (a), (c) and from standard errors derived from GTSM (b), (d) for M_2 amplitudes (a), (b) and M_2 phases (c), (d).

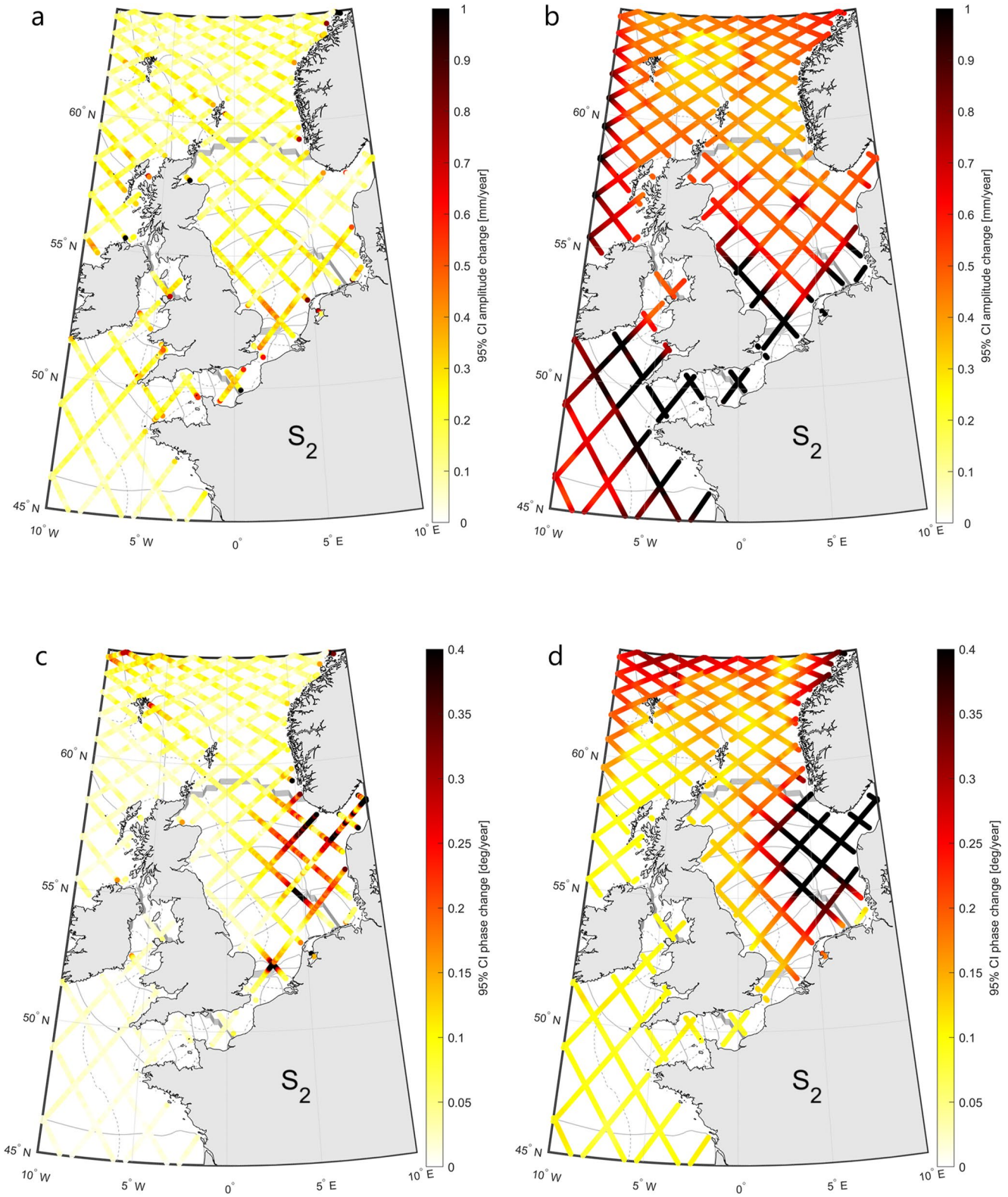

Figure 11. 95% confidence intervals for trend estimates derived from confidence intervals computed by UTide (a), (c) and from standard errors derived from GTSM (b), (d) for S_2 amplitudes (a), (b) and S_2 phases (c), (d).

whereby any correlation between the amplitude and phase estimates was ignored. However, this approach can be carried out with the standard available tidal software and allows a straightforward implementation of non-linear changes. Then, in the second approach (TintHA), the linear change in tidal constants was estimated during the harmonic analysis. This way, the entire time series could be analyzed at once, which reduced the issue of aliasing. In the TintHA approach, no empirical correction for a possible residual nodal modulation was derived. However, results from the SegHA approach suggest this residual to be not significant on global scale (not shown here). Moreover, both methods produced very similar results, both when applied to the sub-sampled tide gauge data (Figure 2) and to the actual satellite radar altimeter data. Due to the rather low magnitudes of secular trends in tides (Figures 4, 5 and 9; Figures S6 and S7 in Supporting Information S1), in many regions the estimated trends just exceed the confidence levels (see Figures 6, 10 and 11; Figures S2 and S3 in Supporting Information S1).

5.1. Satellite-Derived Secular Change in Tides

The main findings presented in this paper are as follows. The amplitudes of the considered tides have changed by up to 1 mm/year over the past ~3 decades. This implies a change of up to 10 cm per century. The change in total tidal range remains unsure because many tidal constituents are not resolvable with the available data. Whether the amplitudes were subject to an increase or a decline varies on a regional (mainly applies to S_2 and K_1) to even local basis (M_2, O_1). On the North West European Shelf, relatively large phase changes are observed close to amphidromic points (Figures 9c and 9d) which may suggest a displacement of these points. This could also be a (partial) explanation for observed variability in changes in amplitude (Figures 9a and 9b), as a displacement of an amphidromic point would reduce the tidal amplitude in the direction of the displacement and increase the amplitude in the opposite direction. This may also explain the differences in the sign of the observed changes on relatively small spatial scales. However, note that from the experiment with tide gauge data it followed that the accuracy of derived phase changes reduces strongly when tidal amplitudes are low (Figures 2b and 2d), which is the case near amphidromic points.

Results have also been compared to trend estimates from tide gauges. However, caution is required. The distance between tide gauges and the nearest TPJ-data exceeds ~50 km in most cases and processes that affect tides near the coast may be very different from those at open sea. Moreover, the estimated trends at crossovers are spatial averages, that may not correspond to the signal that is observed at tide gauges (being point estimates). For M_2, similar secular changes were derived from altimetry and nearby tide gauges along the coast of the Netherlands, France, Denmark and the south of Norway (Figures 9a and 9c). Discrepancies were observed along the west coast of Norway and in shallow waters around the United Kingdom (UK). The former may be related to the Norwegian coastal current and associated mesoscale activity. While the application of the 'mesoscale correction' significantly improved the consistency in trend estimates from crossing tracks, still more inconsistencies are observed in regions where mesoscale variability is also large. In addition, the capricious nature of the coastline (both Norway and UK) may have affected estimates from the altimeter data and/or explain differences between coastal (tide gauge) and shelf estimates (altimeter). Fewer similarities were observed for the S_2 tide. These were predominantly restricted to the Dutch coast. On the global scale, reasonable similarities between secular change derived from tide gauges and altimeter data were observed for S_2 (59%), $O1_2$ (64%) and K_1 (63%) while for M_2, this was only the case for 41% of the tide gauge-crossover combinations. However, such comparisons may be deceptive given the distance between crossovers and the nearest tide gauge (Figure 1a) and significant spatial variability in amplitude change (for M_2 in particular) observed at this distance (Figure 1b). Strictly speaking, the comparison between tide gauge- and TPJ-derived estimates is therefore not a validation, because the estimates refer to different locations.

5.2. UTide- versus GTSM-Derived Confidence Intervals

The presented study considers both uncertainties estimates derived from UTide and computed with GTSM reanalysis data. From a comparison of both products (e.g., Figures 10 and 11) it appears that the uncertainties are most likely underestimated by UTide. In particular on shelf regions, one would expect larger uncertainties due to larger non-tidal residuals and unresolved shallow water tides, while the UTide-derived uncertainties are equally low and homogeneous in shelf regions as on the open ocean. Likely, the application of the 'mesoscale correction' in shallow water removes some tidal signal that is aliased in the SLA product that was used for this correction (Zaron & Ray, 2018). This would reduce the residuals and hence it may have caused too optimistic uncertainty estimates by

UTide. Moreover, from the analysis described in Section 3.3.2, it follows that the confidence intervals estimated by UTide are relatively unaffected by changes in data availability. This also followed from an additional experiment using random subsets of the TPJ-data at crossovers (Text S2 in Supporting Information S1). Comparing Figure 6a and Figure S1b in Supporting Information S1, it appears that the UTide-derived uncertainties are of similar magnitude for the full crossover time series as for half the amount of data, while dividing the data in half may actually cause significant differences in trend estimate (Figure S1a in Supporting Information S1). This finding puts to question the reliability of the UTide-derived confidence intervals. On the other hand, the impact of data availability on the uncertainty is reflected by the GTSM uncertainties (e.g., see Figure 6b and Figure S1c in Supporting Information S1), indicating the added value of this product. Nevertheless, the GTSM-derived uncertainties could for instance not explain all ambiguities at crossing tracks (Figures 9a–9d). In addition, from the comparison of the confidence intervals using tide gauge data (Section 3), both the UTide- and GTSM-derived products appear to underestimate the uncertainties to some extent. However, one should keep in mind that these coastal results cannot directly be transferred to open ocean. For instance, GTSM does not include all physical processes that affect the water level near the coast (e.g., river outflows) and the relation between the spectrum of non-tidal water levels at the coast and on open ocean is unknown. For future studies, we recommend the use of a full 3D model that allows for direct comparison of the observed and reanalysis data. Such a model would include the mesoscale variability that is also present in the satellite radar altimeter data and allow for the same corrections to be applied to both the satellite data and reanalysis data. Moreover, from Figure 3b and Text S2 in Supporting Information S1 it follows that concerning the phase changes, the UTide- and GTSM-derived confidence intervals are more similar and both appear to underestimate the actual uncertainty. The analysis of phase changes on the North West European Shelf suggests that the GTSM-derived confidence intervals in the vicinity of amphidromic points may be too optimistic. This can be explained by the fact that the locations used for the GTSM confidence intervals do not coincide with the TPJ-tracks and/or location of amphidromic points. Ideally, the model-based confidence intervals should be derived at the exact location of the satellite data but this kind of data was not available. Finally, the uncertainty may be reduced by the inclusion of data from other satellite missions. However, given the low magnitude of the observed secular trends, even small intermission biases in the range corrections could be easily mistaken for changes in the actual tides and should thus be taken appropriate care of.

5.3. Potential Secular Changes Introduced by Satellite Data Processing

The magnitude and strong regional variability of the secular change in M_2 amplitudes corresponds to findings by other studies based on tide gauge data (e.g., Müller et al., 2011; Schindelegger et al., 2018; Woodworth, 2010). However, the altimeter-derived change in the S_2 tide differs from some documented findings (e.g., Ray, 2009; Woodworth, 2010). For instance, they found the S_2 amplitudes to have increased along the Gulf of Alaska. This contrasts both to what is derived from altimeter data at open ocean and our analysis of GESLA-3 tide gauge records (Figures 4b and 7b). This suggests that the difference may be related to the differences in considered periods. On the other hand, the inconsistencies may be associated with the atmospheric loading correction (DAC). This correction was applied to TPJ-water levels to reduce the impact of aliasing of non-tidal water level variation on the estimation of tidal harmonic constants. For the sake of consistency, the same correction was applied to the tide gauge data, which is typically not done in earlier studies on tide gauge data. Therefore, a possible S_2-like signal in DAC (for instance related to the six-hour resolution of the product) may have affected the results.

More general, it is possible that any systematic error or secular change in the atmospheric propagation (wet/dry troposphere and ionosphere) or reference frame corrections could have affected the trend estimates derived from the water levels. According to Zawadzki et al. (2018), estimation of the S_2 tide is particular sensitive to (errors in) the geophysical/range corrections. Additional trend analysis of the individual corrections suggest limited influence on M_2 and O_1 (Figures S8 and S11 in Supporting Information S1). Only the wet troposphere correction shows secular change in the amplitudes of up to 0.15 mm/year. The magnitude of these changes is low compared to the trend in the water level (~1 mm/year) and the computed correlation is insignificant. Larger signals are observed for S_2 (Figure S9 in Supporting Information S1; up to 0.25 mm/year). However, none of these signals show significant correlation with the secular change derived from the water levels. In addition, a possible effect from errors in the (model-derived) ionospheric correction on the S_2 tide was already incorporated in the confidence intervals for this tide (Text S1 in Supporting Information S1). Some K_1 signal is observed in the wet troposphere and altimeter derived ionosphere correction. However, again, the correlation with water level-derived change is low (<0.1) and positive. Since the corrections are subtracted from the range to obtain the

water level, only a negative correlation would explain the secular change derived from the water levels. Finally, there may be intermission biases in range corrections that could be partly responsible for the observed trend in S_2 amplitudes, such as the CG-correction that was applied to TOPEX/Poseidon data (Beckley et al., 2021; Zawadzki et al., 2018). All in all, the analysis of the S_2 remains tricky and a more thorough analysis is deemed necessary.

5.4. Explaining the Observed Secular Changes by Means of Physical Processes

The results presented in this paper merely allow speculation about the drivers behind the observed trends. The strong local variability in some areas suggests that local processes may dominate there or that the observed change is in fact related to internal tide variability. For instance, Zhao (2016) showed that in several regions, the propagation of the internal tidal wave is subject to interannual or decadal variability. This causes temporal differences in the phase of the internal tide that increase as the internal tide propagates. Since the tidal amplitude that is observed at the surface is a combination of the barotropic and internal tide, its value depends on the phase difference between the two. As mentioned, the interannual change in these phase differences can vary as the internal tide travels further from its origin, which may cause an apparent increase in observed tidal amplitude at one crossover, but a decrease at the next. Regions where significant small-scale variability in trend estimates is observed (e.g., 30°S, 160°W; 20°N, 30°W; 15°S, 50°E), correspond to locations where the amplitude of the internal M_2 amplitude is rather high (Zhao, 2016). On the other hand, regions where the internal M_2 amplitude is low (i.e., equatorial Pacific) correspond to regions where spatial variability in yearly change in M_2 amplitude is also low.

On the other hand, part of the observed signal could be related to sea ice decline (see e.g., Haigh et al., 2020). Namely, the observed changes in M_2 amplitude around Iceland (Figure 4a) are of opposite sign compared to the March-September amplitude differences documented by Bij de Vaate et al. (2021). This indicates that over time the annual average tide becomes closer to the September case, which is in line with interannual sea ice decline. This may also explain the increased spatial correlation in observed trends in M_2 amplitudes near the poles. Furthermore, changes in tides have been linked to sea level rise. For instance, the modeled effect of SLR on M_2 amplitudes was found to be ∼10 cm/m SLR (e.g., Pickering et al., 2017; Schindelegger et al., 2018). This, given a SLR of ∼3 mm/year since 1990, is of comparable magnitude to the TPJ-derived amplitude changes in most regions (∼0.3 mm/year). However, the modeled M_2 amplitude change under the influence of SLR does not exhibit the large regional variability that was seen in the altimetry-derived trends, although a number of similarities can be observed on for instance the North West European Shelf. On another note, the zonal pattern in the S_2 amplitude change is striking and not as strong for the other (lunar) tides. If the observed change is in fact related to the tide and not to other non-tidal processes, this suggests the causes may be related to radiational forcing. About 15% of the S_2 tide is driven by pressure loading of the ocean (Haigh et al., 2020) and interannual variability in atmospheric pressure could translate into variable S_2 amplitudes. Given that atmospheric pressure fluctuates continuously (Lu & Tu, 2021), it may be that the secular change in S_2 amplitude cannot be accurately described by a linear trend. Finally, although we can at this stage not draw conclusions on the drivers behind the observed changes in tides, our findings could be useful for future (modeling) studies on this phenomenon.

Data Availability Statement

Tide gauge data were kindly provided by the Agentschap Maritieme Dienstverlening en Kust, Belgium; Danish Coastal Authority; Danish Meteorological Institute; Danish Maritime Safety Administration; Service Hydrographique et Océanographique de la Marine, France; Die Wasserstraßen-und Schifffahrtsverwaltung des Bundes, Germany; Rijkswaterstaat, Netherlands; Norwegian Hydrographic Service, and U.K. National Tidal and Sea Level Facility (NTSLF). The reanalysis data (GTSM) were kindly provided by Deltares, Netherlands. The UTide software was obtained through https://www.mathworks.com/matlabcentral/fileexchange/46523-utide-unified-tidal-analysis-and-prediction-functions. The GESLA-3 data set is located on https://doi.org/10.1002/gdj3.174, the DUACS SLA product is located on https://doi.org/10.48670/moi-00148 and the satellite radar altimetry data can be retrieved through the RADS (http://rads.tudelft.nl). The estimated secular trends from TPJ-data are made available here: https://doi.org/10.4121/17086394.

Acknowledgments
This work is part of the research programme FAST4NI with project number ALWPP.2017.001, which is (partly) financed by the Dutch Research Council (NWO).

References

Beckley, B., Ray, R. D., Zelensky, N., Lemoine, F., Brown, S., Desai, S., & Mitchum, G. (2021). Integrated multi-mission Ocean altimeter data for climate research TOPEX/Poseidon. *Jason-1, 2, 3 User's Handbook Version 5.1*.

Bij de Vaate, I., Vasulkar, A. N., Slobbe, D. C., & Verlaan, M. (2021). The influence of Arctic Landfast ice on seasonal modulation of the M2 tide. *Journal of Geophysical Research: Oceans*, *126*, e2020JC016630. https://doi.org/10.1029/2020jc016630

Cartwright, D. E., & Edden, A. C. (1973). Corrected tables of tidal harmonics. *Geophysical Journal of the Royal Astronomical Society*, *33*, 253–264. https://doi.org/10.1111/j.1365-246X.1973.tb03420.x

Cartwright, D. E., & Taylor, R. J. (1971). New computations of the tide-generating potential. *Geophysical Journal of the Royal Astronomical Society*, *23*, 45–73. https://doi.org/10.1111/j.1365-246X.1971.tb01803.x

Cherniawsky, J. Y., Foreman, M. G., Kang, S. K., Scharroo, R., & Eert, A. J. (2010). 18.6-year lunar nodal tides from altimeter data. *Continental Shelf Research*, *30*(6), 575–587. https://doi.org/10.1016/j.csr.2009.10.002

Codiga, D. L. (2011). *Unified tidal analysis and prediction using the UTide Matlab functions. Technical report 2011-01*. Graduate School of Oceanography, University of Rhode Island.

Codiga, D. L. (2020). UTide unified tidal analysis and prediction functions [Software]. MATLAB Central File Exchange. Retrieved from https://www.mathworks.com/matlabcentral/fileexchange/46523-utide-unified-tidal-analysis-and-prediction-functions

Dangendorf, S., Calafat, F. M., Arns, A., Wahl, T., Haigh, I. D., & Jensen, J. (2014). Mean sea level variability in the North Sea: Processes and implications. *Journal of Geophysical Research: Oceans*, *119*(10). https://doi.org/10.1002/2014jc009901

Devlin, A. T., Jay, D. A., Talke, S. A., Zaron, E. D., Pan, J., & Lin, H. (2017). Coupling of sea level and tidal range changes, with implications for future water levels. *Scientific Reports*, *7*(1), 1—12. https://doi.org/10.1038/s41598-017-17056-z

Foreman, M. G. G. (2004). Manual for tidal heights analysis and prediction, revised. *Pacific Marine Science Report*, *77*, 10.

Guarneri, H., Verlaan, M., Slobbe, D. C., Veenstra, J., Bij de Vaate, I., & Afrasteh, Y. (2022). Estimating tides from satellite radar altimetry in coastal seas. *Marine Geodesy*. (Manuscript in preparation).

Hagen, R., Plüß, A., Jänicke, L., Freund, J., Jensen, J., & Kösters, F. (2021). A combined modeling and measurement approach to assess the nodal tide modulation in the North Sea. *Journal of Geophysical Research: Oceans*, *126*, e2020JC016364. https://doi.org/10.1029/2020jc016364

Haigh, I. D., Marcos, M., Talke, S. A., Woodworth, P. L., Hunter, J. R., Haugh, B. S., et al. (2021). GESLA version 3: A major update to the global higher-frequency sea-level dataset [Dataset]. Geoscience Data Journal. https://doi.org/10.1002/gdj3.174

Haigh, I. D., Pickering, M. D., Green, J. M., Arbic, B. K., Arns, A., Dangendorf, S., et al. (2020). The tides they are a-Changin': A comprehensive review of past and future nonastronomical changes in tides, their driving mechanisms, and future implications. *Reviews of Geophysics*, *58*(1), e2018RG000636. https://doi.org/10.1029/2018rg000636

Hinton, A. C. (2000). Tidal changes and coastal hazards: Past, present and future. *Natural Hazards*, *21*(2), 173–184. https://doi.org/10.1023/a:1008131002450

Jee, G., Lee, H. B., Kim, Y. H., Chung, J. K., & Cho, J. (2010). Assessment of GPS global ionosphere maps (GIM) by comparison between CODE GIM and TOPEX/Jason TEC data: Ionospheric perspective. *Journal of Geophysical Research*, *115*(A10). https://doi.org/10.1029/2010ja015432

Jin, G., Pan, H., Zhang, Q., Lv, X., Zhao, W., & Gao, Y. (2018). Determination of harmonic parameters with temporal variations: An enhanced harmonic analysis algorithm and application to internal tidal currents in the South China Sea. *Journal of Atmospheric and Oceanic Technology*, *35*(7), 1375–1398. https://doi.org/10.1175/jtech-d-16-0239.1

Khojasteh, D., Glamore, W., Heimhuber, V., & Felder, S. (2021). *Sea level rise impacts on estuarine dynamics: A review*. Science of the Total Environment, 146470.

Li, S., Wahl, T., Talke, S. A., Jay, D. A., Orton, P. M., Liang, X., et al. (2021). Evolving tides aggravate nuisance flooding along the US coastline. *Science Advances*, *7*(10), eabe2412. https://doi.org/10.1126/sciadv.abe2412

Lu, E., & Tu, J. (2021). Relative importance of surface air temperature and density to interannual variations in monthly surface atmospheric pressure. *International Journal of Climatology*, *41*, E819–E831. https://doi.org/10.1002/joc.6730

Mercator Ocean International. (2021). GLOBAL OCEAN GRIDDED L4 SEA SURFACE HEIGHTS AND DERIVED VARIABLES REPROCESSED (1993-ONGOING) [Dataset]. Mercator Ocean International. https://doi.org/10.48670/MOI-00148

Müller, M. (2012). The influence of changing stratification conditions on barotropic tidal transport and its implications for seasonal and secular changes of tides. *Continental Shelf Research*, *47*, 107–118. https://doi.org/10.1016/j.csr.2012.07.003

Müller, M., Arbic, B. K., & Mitrovica, J. X. (2011). Secular trends in ocean tides: Observations and model results. *Journal of Geophysical Research*, *116*(C5).

Müller, M., Cherniawsky, J. Y., Foreman, M. G. G., & Von Storch, J. S. (2014). Seasonal variation of the M 2 tide. *Ocean Dynamics*, *64*(2), 159–177. https://doi.org/10.1007/s10236-013-0679-0

Naeije, M. (2020). Radar Altimeter Database System [Data archive]. DEOS. Retrieved from http://rads.tudelft.nl

Pawlowicz, R., Beardsley, B., & Lentz, S. (2002). Classical tidal harmonic analysis including error estimates in MATLAB using T-TIDE. *Computers & Geosciences*, *28*, 929–937. https://doi.org/10.1016/s0098-3004(02)00013-4

Pickering, M. D., Horsburgh, K. J., Blundell, J. R., Hirschi, J. M., Nicholls, R. J., Verlaan, M., & Wells, N. C. (2017). The impact of future sea-level rise on global tides. *Continental Shelf Research*, *142*, 50–68. https://doi.org/10.1016/j.csr.2017.02.004

Ray, R. D. (2009). Secular changes in the solar semidiurnal tide of the Western North Atlantic Ocean. *Geophysical Research Letters*, *36*(29), 108–116. https://doi.org/10.1029/2009gl040217

Ray, R. D. (2016). On measurements of the tide at Churchill, Hudson Bay. *Atmosphere-Ocean*, *54*(2), 108–116. https://doi.org/10.1080/07055900.2016.1139540

Ray, R. D. (2020). Daily harmonics of ionospheric total electron content from satellite altimetry. *Journal of Atmospheric and Solar-Terrestrial Physics*, *209*, 105423. https://doi.org/10.1016/j.jastp.2020.105423

Ray, R. D., & Zaron, E. D. (2016). M_2 internal tides and their observed wavenumber spectra from satellite altimetry. *Journal of Physical Oceanography*, *46*(1), 3–22. https://doi.org/10.1175/jpo-d-15-0065.1

Ross, A. C., Najar, R. G., Li, M., Lee, S. B., Zhang, F., & Liu, W. (2017). Fingerprints of sea level rise on changing tides in the Chesapeake and Delaware Bays. *Journal of Geophysical Research: Oceans*, *122*, 8102–8125. https://doi.org/10.1002/2017JC012887

Rousseeuw, P. J., & Croux, C. (1993). Alternatives to the median absolute deviation. *Journal of the American Statistical Association*, *88*(424), 1273–1283. https://doi.org/10.1080/01621459.1993.10476408

Savcenko, R., & Bosch, W. (2007). Residual tide analysis in shallow water-contributions of ENVISAT and ERS altimetry. ESA-SP636 (CD-ROM). *Proceedings of the Envisat Symposium*.

Scharroo, R., Leuliette, E. W., Naeije, M. C., Martin-Puig, C., & Pires, N. (2016). RADS version 4: An efficient way to analyse the multi-mission altimeter database. *Proceedings of the ESA Living Planet Symposium*, *9–13*. (ESA Special Publication SP-740).

Schindelegger, J. A. M., Green, M., Wilmes, S. B., & Haigh, I. D. (2018). Can we model the effect of observed sea level rise on tides? *Journal of Geophysical Research: Oceans*, *123*, 4593–4609. https://doi.org/10.1029/2018jc013959

Schrama, E. J. O., & Ray, R. D. (1994). A preliminary tidal analysis of TOPEX/POSEIDON altimetry. *Journal of Geophysical Research*, *99*(C12), 24799–24808. https://doi.org/10.1029/94jc01432

St-Laurent, P., Saucier, F. J., & Dumais, J. F. (2008). On the modification of tides in a seasonally ice-covered sea. *Journal of Geophysical Research*, *113*(11), 1–11. https://doi.org/10.1029/2007JC004614

Taburet, G., Sanchez-Roman, A., Ballarotta, M., Pujol, M. I., Legeais, J. F., Fournier, F., et al. (2019). Duacs DT2018: 25 years of reprocessed sea level altimetry products. *Ocean Science*, *15*(5), 1207–1224. https://doi.org/10.5194/os-15-1207-2019

Wahr, J. M. (1985). Deformation induced by polar motion. *Journal of Geophysical Research*, *90*(B11), 9363–9368. https://doi.org/10.1029/JB090iB11p09363

Wang, X., Verlaan, M., Apecechea, M. I., & Lin, H. X. (2021). Computation-efficient parameter estimation for a high-resolution global tide and Surge model (GTSM). *Journal of Geophysical Research: Oceans*, *126*, e2020JC016917. https://doi.org/10.1029/2020JC016917

Woodworth, P. L. (2010). A survey of recent changes in the main components of the ocean tide. *Continental Shelf Research*, *30*(15), 1680–1691. https://doi.org/10.1016/j.csr.2010.07.002

Zaron, E. D., & Jay, D. A. (2014). An analysis of secular change in tides at open-ocean sites in the Pacific. *Journal of Physical Oceanography*, *44*(7), 1704–1726. https://doi.org/10.1175/jpo-d-13-0266.1

Zaron, E. D., & Ray, R. D. (2018). Aliased tidal variability in mesoscale sea level anomaly maps. *Journal of Atmospheric and Oceanic Technology*, *35*(12), 2421–2435. https://doi.org/10.1175/jtech-d-18-0089.1

Zawadzki, L., Ablain, M., Carrere, L., Ray, R. D., Zelensky, N. P., Lyard, F., et al. (2018). Investigating the 59-day error signal in the mean sea level derived from TOPEX/Poseidon, Jason-1, and Jason-2 data with FES and GOT ocean tide models. *IEEE Transactions on Geoscience and Remote Sensing*, *56*(6), 3244–3255. https://doi.org/10.1109/tgrs.2018.2796630

Zhao, Z. (2016). Internal tide oceanic tomography. *Geophysical Research Letters*, *43*(17), 9157–9164. https://doi.org/10.1002/2016gl070567

References From the Supporting Information

Fernandes, M. J., Lázaro, C., Nunes, A. L., & Scharroo, R. (2014). Atmospheric corrections for altimetry studies over inland water. *Remote Sensing*, *6*(6), 4952–4997.